View metadata, citation and similar papers at core.ac.uk
brought to you by CORE
provided by NASA Technical Reports Server

N94-31434

A STUDY OF THE SPACE STATION '*FREEDOM*' RESPONSE TO THE DISTURBANCE ENVIRONMENT

A. Suleman,* V.J. Modi,** and V.B. Venkayya ***

Flight Dynamics Directorate
Wright Laboratory, WL/FIBR
Wright-Patterson AFB OH 45433-6553

ABSTRACT

A relatively general formulation for studying the dynamics and control of an arbitrary spacecraft with interconnected flexible bodies has been developed[1]. This self-contained and comprehensive numerical algorithm using system modes is applicable to a large class of spacecraft configurations of contemporary and future interests. Here, versatility of the approach is demonstrated through the dynamics and control studies aimed at the evolving Space Station *Freedom*.

1. INTRODUCTION

The next generation of communications satellites, Space Shuttle based experiments, proposed Space Station *Freedom*, and many others belong to a class of systems which are large and flexible, and their analysis is amenable only to numerical simulation requiring efficient algorithms. A challenge faced by engineers is to simulate the dynamics and control of such systems using accurate mathematical models.

Given the large size of these orbiting systems and the expected growth from the initial operational configuration, the structural flexibility will be a key parameter governing their dynamical behaviour. The presence of environmental and operational disturbances will only add to the complexity of the problem. Hence thorough understanding of interactions between librational dynamics, flexibility, inertia and orbital parameters as well as initial disturbances is of importance.

With this as background, the paper presents a rather self-contained and comprehensive numerical algorithm for simulating dynamical behaviour of large space structures. Here, its versatility is demonstrated through the dynamics and control studies aimed at the evolving Space Station *Freedom* (Figure 1).

---

* NRC Research Associate
** Professor, University of B.C., Vancouver, Canada
*** Principal Scientist

2. MULTIBODY DYNAMICS FORMULATION

Having recognized the importance of flexibility, particularly with reference to large evolving space structures, there have been considerable effort aimed at general multibody formulations applicable to a wide class of flexible systems. The models considered vary significantly; however, the underlying objective is to obtain dynamic equations of motion for a system of arbitrarily connected flexible members in a branched or closed loop topological form.

The amount of time and effort involved in derivation of the equations of motion are indeed significant. The resulting kinetic and kinematic expressions as well as the governing equations of motion are quite lengthy even in matrix notation. The Lagrangian formulation has the following distinctive features:

(a) it is applicable to an arbitrary number of beam, plate, membrane and rigid body members, in any desired orbit, interconnected to form an open branch-type topology (Figure 2);

(b) rigid joints between the flexible members permit arbitrary large angle rotation and linear translation between the structural components;

(c) the formulation accounts for the gravity gradient potential, the effects of transient system inertias and shift in the centre of mass;

(d) the flexible character of the system is described by three-dimensional system modal functions obtained using the finite element method;

(e) symbolic manipulation is used to synthesize the equations of motion thus providing a general and efficient modelling capability with optimum allocation of computer resources;

(f) the governing equations are programmed in a modular fashion to isolate the effects of appendage slewing and translation, librational dynamics, structural flexibility and orbital parameters;

(g) operational disturbances (Space Shuttle docking, crew motion and maintenance operation maneuvers) have been implemented in this dynamic simulation tool. Other disturbances can easily be incorporated through generalized forces and initial conditions;

(h) both the nonlinear and linear forms of the equations of motion have been formulated to permit assessment of a wide variety of control strategies, both linear and nonlinear.

The governing equations of motion can be obtained from

$$\frac{d}{dt}\left(\frac{\partial T}{\partial \dot{\bar{q}}}\right) - \frac{\partial T}{\partial \bar{q}} + \frac{\partial U}{\partial \bar{q}} = \bar{F}_q \,,$$

where $\bar{q}$ and $\bar{F}_q$ represent the generalized coordinates and associated forces, respec-

tively. The above equations can be rewritten in vector form as

$$\mathbf{M}(\bar{q})\,\bar{q}'' = \begin{Bmatrix} \bar{Q}_\theta \\ \\ \bar{Q}_p \end{Bmatrix},$$

where:

$$\bar{Q}_\theta = \frac{d}{dt}\Big(\frac{\partial \overline{\omega}^T}{\partial \dot{\bar{\theta}}}\Big)\,\mathbf{I}\,\overline{\omega} - \frac{\partial \overline{\omega}}{\partial \bar{\theta}}\frac{d}{dt}\,\mathbf{I}\,\overline{\omega} - \frac{\partial \overline{\omega}^T}{\partial \dot{\bar{\theta}}}\,\mathbf{I}\,\frac{d\overline{\omega}}{dt} - \frac{d}{dt}\Big(\frac{\partial \overline{\omega}^T}{\partial \dot{\bar{\theta}}}\Big)\,\bar{H}$$
$$- \frac{\partial \overline{\omega}^T}{\partial \dot{\bar{\theta}}}\,\frac{d\overline{H}}{dt} + \frac{\partial \overline{\omega}^T}{\partial \bar{\theta}}\,\mathbf{I}\,\overline{\omega} + \frac{\partial \overline{\omega}^T}{\partial \bar{\theta}}\,\overline{H} + \frac{\partial U}{\partial \bar{\theta}}\,;$$

$$\bar{Q}_p = -\frac{d}{dt}\Big(\frac{\partial \sum T_i}{\partial \dot{\bar{p}}}\Big) - \frac{d}{dt}\Big(\frac{\partial \overline{H}}{\partial \dot{\bar{p}}}\Big)^T \overline{\omega} - \Big(\frac{\partial \overline{H}}{\partial \dot{\bar{p}}}\Big)^T \frac{d\overline{\omega}}{dt}$$
$$+ \frac{\partial \sum T_i}{\partial \bar{p}} + \frac{1}{2}\,\overline{\omega}^T \frac{\partial \mathbf{I}}{\partial \bar{p}}\,\overline{\omega} + \Big(\frac{\partial \overline{H}}{\partial \bar{p}}\Big)\,\overline{\omega} + \frac{\partial U}{\partial \bar{p}}\,.$$

Here $\mathbf{M}(\bar{q})$ represents the nonlinear mass matrix, while $\bar{Q}_\theta$ and $\bar{Q}_p$ correspond to the nonlinear stiffness, gyroscopic and forcing terms for the librational and vibrational degrees of freedom, respectively. $\overline{H}$ is the angular momentum with respect to the orbital frame; $\overline{\omega}$, the librational velocity vector; $\mathbf{I}$, the inertia matrix; and $\sum T_i$; the total kinetic energy due to the structural flexibility. The vector $\bar{q}$ is comprised of two vectors, $\bar{\theta}$ and $\bar{p}$, where $\bar{\theta} = \{\psi, \phi, \lambda\}$ for the librational degrees of freedom and $\bar{p} = \{p_1, p_2, ..., p_n\}$ for the vibrational degrees of freedom.

3. ATTITUDE CONTROL METHODOLOGY

Nonlinear control has received considerable attention in the past decade, particularly in the robotics applications. Linear control techniques based on either the Bellman's principle of optimality or on the Pontryagin's maximum principle, fail to provide reliable and accurate results, particularly when the nonlinearities of the system become important. To overcome this limitation, Freund[2] proposed the use of the state feedback to decouple the nonlinear system in such a way that an arbitrary placement of poles becomes possible.

Inverse control, based on the Feedback Linearization Technique (FLT), was first investigated by Beijczy[3] and used by Singh and Schy[4] for control of a rigid arm robot. Spong and Vidyasagar[5] also used the FLT to formulate a control procedure for rigid manipulators. Given a dynamical model of the system, the controller first utilizes the feedback to linearize the system followed by a linear compensator to achieve the desired output. Here, the FLT is applied to the FMC of the Space Station to achieve attitude control in the presence of structural flexibility.

3.1 Feedback Linearization Technique

This procedure has been applied with success in many control problems dealing with rigid systems. A particular application is in the trajectory tracking of a given structure where the dynamics involves only the rigid modes. For example, consider a system described by a set of equations in the form

$$\mathbf{M}(\bar{\theta},t)\ddot{\bar{\theta}} + \bar{F}(\bar{\theta},\dot{\bar{\theta}},t) = \bar{Q}_{\bar{\theta}}(\dot{\bar{\theta}},\bar{\theta},t), \tag{1}$$

where the generalized coordinate vector accounts only for the rigid degrees of freedom. The objective is to seek a nonlinear feedback control $\bar{Q}_{\bar{\theta}}(\dot{\bar{\theta}},\bar{\theta},t)$, which when substituted in the above equation leads to a linear closed loop system. It has been shown[6] that, the resulting system becomes asymptotically stable around the nominal trajectory if the driving control efforts are given by

$$\bar{Q}_{\bar{\theta}} = \mathbf{M}(\bar{\theta},t)\bar{v} + \bar{F}(\bar{\theta},\dot{\bar{\theta}},t),$$

where

$$\ddot{\bar{\theta}}_d + \mathbf{K}_v(\dot{\bar{\theta}}_d - \dot{\bar{\theta}}) + \mathbf{K}_p(\bar{\theta}_d - \bar{\theta}) = \bar{v}, \tag{2}$$

and $\bar{\theta}_d$, $\dot{\bar{\theta}}_d$ and $\ddot{\bar{\theta}}_d$ correspond to the desired trajectory characteristics. Here $\mathbf{K}_p$ and $\mathbf{K}_v$ are the 3×3 matrices of position and velocity feedback gains, respectively. They are so chosen as to insure stable behaviour of the tracking error, $\bar{e} = \bar{\theta} - \bar{\theta}_d$, given by

$$\ddot{\bar{e}} + \mathbf{K}_v\dot{\bar{e}} + \mathbf{K}_p\bar{e} = \mathbf{0}. \tag{3}$$

A suitable choice for $\mathbf{K}_p$ and $\mathbf{K}_v$ is

$$\mathbf{K}_p = diag\{\chi_1^2,...,\chi_n^2\}; \mathbf{K}_v = diag\{2\chi_1,...,2\chi_n\},$$

where χ_i and ζ represent the controller frequency and damping ratio, respectively. This results in a globally decoupled system with each generalized coordinate responding as a second-order damped oscillator. The natural frequencies χ_i determine the speed of response of the corresponding generalized coordinates. A larger value of χ_i gives rise to a faster response of of the ith degree of freedom.

Recently, Karray and Modi[7] have extended the FLT to include structural flexibility for a model of an orbiting manipulator system. The basic idea here is to design a controller capable of transforming the rigid part of the dynamics into a canonical, decoupled state space model. This, obviously, implies a completely controllable system. Note, here the state of the system is not transformed through a diffeomorphic mapping; rather it is the control effort that makes the rigid part of the system behave as if it were completely linear. Also it is important to notice that if the system were not in the form similar to that in Eq. (1), then a diffeomorphic transformation and a special form of the control effort are needed for reducing the system to the canonical form.

Now, if the observable states are chosen to be the components of the rigid mode subvector $\bar{\theta}$, then by selecting a suitable control vector $\bar{Q}_\theta$, the linearized equations of motion become

$$\ddot{\bar{\theta}}(\psi, \phi, \lambda) = \bar{v},$$

where:

$$\bar{Q}_{\bar{\theta}} = \tilde{\mathbf{M}}\bar{v} + \tilde{\bar{F}},$$

with

$$\tilde{\mathbf{M}} = [\mathbf{M}_{\theta,\theta} - \mathbf{M}_{p,\theta}^T \mathbf{M}_{p,p}^{-1} \mathbf{M}_{p,\theta}]; \qquad \tilde{\bar{F}} = [\bar{F}_\theta - \mathbf{M}_{p,\theta}^T \mathbf{M}_{p,p}^{-1} \bar{F}_p];$$

and $\bar{v}$ takes the form given in Eq. (2). The control effort can be expressed as the sum of two parts, $\bar{Q}_{\theta_1}$ (primary) and $\bar{Q}_{\theta_2}$ (secondary):

$$\bar{Q}_{\theta_1} = \tilde{\mathbf{M}}\ddot{\bar{\theta}}_d + \tilde{\bar{F}}; \qquad \bar{Q}_{\theta_2} = \tilde{\mathbf{M}}(\mathbf{K}_v \dot{\bar{e}} + \mathbf{K}_d \bar{e}).$$

The primary controller is so designed as to compensate for the nonlinear effects corresponding to rigid part of the system. In practice, the system properties and the dynamical model are usually not precisely known. To account for modelling uncertainties, i.e. to impart robust character, a secondary controller $\bar{Q}_\theta$ is introduced. The function of the primary controller is to offset the nonlinear effects inherent in the attitude degrees of freedom; whereas the secondary controller ensures robust behaviour of the error. The question of flexible modes which interact with the rigid ones through $\mathbf{M}_{\theta,p}$ still remains as they are needed for computation of the control effort Q_θ. Two different control schemes are proposed to that end: one leads to a Quasi-Open Loop Control (QOLC) procedure; while the other is termed the Quasi-Closed Loop Control scheme.

3.2 Quasi-Open Loop Control

The central idea here is to evaluate flexibility generalized coordinates through an off-line procedure, i.e., dynamics of the $\bar{p}$ is computed independent of $\bar{\theta}$ (Figure 3a). However, it is still governed by the desired trajectory specified for the rigid degrees of freedom as characterized by $\ddot{\bar{\theta}}_d$, $\dot{\bar{\theta}}_d$ and $\bar{\theta}_d$. Thus the dynamics of $\bar{p}$ evolves according to

$$\ddot{\bar{p}} = -\mathbf{M}_{p,p}^{-1}\{\mathbf{M}_{p,\theta}\bar{v} + \bar{F}_p(\bar{\theta}_d, \dot{\bar{\theta}}_d, \bar{p}, \dot{\bar{p}})\}.$$

Integration of this set of equations, which can be carried out off-line, permits the designer to assess the evolving behaviour of $\bar{p}$ and $\dot{\bar{p}}$, and compute the control effort $\bar{Q}_\theta$ with the tracking error vector governed by Eq. (3). Of course, this implies the dynamics of the flexible generalized coordinates to be stable for the control study. It is important to recognize that the choice of $\bar{v}$ as in Eq. (2), instead of being simply $\ddot{\bar{\theta}}_d$, gives the system a more robust behaviour, similar to that attained with a proportional plus derivative controller.

3.3 Quasi-Closed Loop Control

Here, responses in the rigid and flexible degrees of freedom are computed simultaneously according to the following dynamical relations:

$$\ddot{\bar{\theta}} = \bar{v}$$

$$\ddot{\bar{p}} = -\mathbf{M}_{p,p}^{-1}\{\mathbf{M}_{p,\theta}\bar{v} + \bar{F}_p(\bar{\theta}, \dot{\bar{\theta}}, \bar{p}, \dot{\bar{p}})\}.$$

Now $\bar{F}_p$ is a function of $\bar{\theta}$ and $\dot{\bar{\theta}}$ instead of being governed by $\bar{\theta}_d$ and $\dot{\bar{\theta}}_d$ (Figure 3b). The disadvantage of the scheme is the relatively large computational effort as compared to QOLC. However, the QCLC is less sensitive to system uncertainties.

4. RESPONSE TO OPERATIONAL DISTURBANCES

A study of the First Milestone Configuration (FMC) was undertaken to assess effects of operational disturbances on the system response. Objective was to predict acceleration levels imposed on the station during the operational maneuvers leading to unacceptable dynamics in terms of pitch, roll and yaw response; vibrational displacements, velocities and acceleration profiles at various locations on the Space Station; and torque demands by the controller.

4.1 Nominal Configuration

The first forty system modes (including the six rigid body modes) for the First Milestone Configuration (FMC) were obtained to represent the structural flexibility of the continuous system.

The frequency spectrum provides the free vibration frequencies and associated system modes. The mode characterization helps appreciate the relative contributions of different parts of the Station to each system modal frequency.

In general, modal displacements fall into the following three categories:

(a) Solar Array Deformation Modes: these are the modes in which the solar arrays deform significantly in and out of the X-Y plane as cantilever plates and the remainder of the Station responds only slightly so as to maintain the dynamic equilibrium. Modes which are dominated by the twisting motion of the array plates are also included in this category.

(b) Radiator Modes: These are associated with the PV radiator deformations, which has designed to have a fundamental bending frequency of 0.1 Hz.

(c) Stinger/RCS Boom Coupled Modes: these components are designed to have a fundamental bending frequency of 0.5 Hz, so they appear in combination in the system modes.

(c) Overall System Modes: in general, these modes involve an overall motion of the Station, with solar array and radiator deformations coupled with response of the main truss in and out of the X-Y and X-Z planes.

For the earlier proposed FMC, the appendage response in bending dominated the first six elastic modes ($f_7 - f_{12}$) with frequencies in the range of 0.1 - 0.5 Hz (Figure 4). Of these, the first three modes (f_7, f_8, f_9) pertain to the PV array and radiator while $f_{10} - f_{12}$ correspond to the RCS boom and stinger assembly. It is of interest to recognize that the torsional motion of the main truss is represented by f_9 while the corresponding bending in Z and Y directions correspond to $f_{21} = 2.30$ Hz and $f_{22} = 2.35$ Hz, respectively. Note, the stinger and RCS boom motions are coupled as both have a fundamental frequency of 0.5 Hz. On the other hand, the PV arrays and radiators have their fundamental component frequency of 0.1 Hz as cantilevers. The solar array deformation modes display pure torsional motion in symmetric and asymmetric modes at f_{16} and f_{17} (1.14 Hz) with higher harmonics represented by f_{24}, f_{25} (2.4 Hz) and f_{31}, f_{32} (5.97 Hz).

4.2 Solar Array Sun Tracking

The Space Station attitude orientation will be in the Local Vertical-Local Horizontal (LVLH) mode, with its main truss along the local horizontal and the solar arrays perpendicular to the orbital plane. The arrays are provided with the rotational capability, about the alpha and beta joints, in order to track the sun for optimum exposure. Another design objective, which will require rotation of the solar panels, is to maintain a "feathered" flight configuration in order to reduce the aerodynamic drag. Obviously, changes in the orientation of the solar panels due to these maneuvers will affect structural flexibility characteristics of the Space Station and the associated frequency spectrum. The rotational rates of the solar panels are relatively slow, such that a quasi-static condition prevails during the maneuver.

For a 90° rotation of the solar panels about the α-joint (Figure 5a), the frequency spectrum undergoes significant changes, particularly at modes 16, 18, 19, 25, 27, 29 and 33, with variations as large as 35% in mode 16. Analysing the modal displacements, mode 27 starts with the solar arrays undergoing torsional motion, and as the maneuver progresses, the deformations become predominant in bending. Similar changes in the behaviour were observed in other modes as well. For instance, mode 18 exhibited main truss bending about Y-axis coupled with solar array bending at the start of the maneuver,and by the end, the structural response was characterized entirely by the torsional motion of the arrays. Also of interest is the interchange of modal energy among the modes and between the components in the same mode. For mode 29, large bending displacements of the solar panels coupled with slight bending of the radiator, stinger and RCS boom were observed in the nominal configuration. By the end of the maneuver, the radiator exhibits large modal displacements with a small motion of the solar arrays.

This information is utilized in the multibody dynamics simulations such that the modes are updated, so as to maintain an accurate representation of the flexibility of the system during the maneuver. The simulation is carried out for 0.25 orbit

(25 minutes), with a total array rotation of 90° at an angular velocity $\dot{\Theta}$. The modes are updated at 15° intervals and the nonlinear controller gains are based on $\chi = 10^{-2}\, rad/s$ and $\zeta = 1$.

Figure 5b shows the dynamical response of the FMC. The control effort to maintain the Station in the LVLH orientation is minimal, with the peak $Q_\psi = 1.4$ Nm and $Q_\lambda = Q_\phi = 0.5$ Nm. Since the controller is commanded to drive the system to the LVLH orientation, which is not a Torque Equilibrium Attitude (TEA) position ($\psi_e = 1.5°, \lambda_e = \phi_e = 0°$), the control effort in the pitch degree of freedom continues to persist at an average level of 1 Nm.

Of interest is the transfer of energy between the be seen that a transfer of energy is taking place. At perigee, the beginning of the maneuver, the solar panel tip deflection is larger than the PV radiator (3×10^{-4} and 3×10^{-5} m, respectively. At the end of the maneuver, when the spacecraft has completed 0.25 orbits, the PV radiator appears to contain most of the modal energy, with the tip displacement considerably higher than that of the solar panel. The main truss displacement at the modules location increases during the maneuver, while the microgravity levels stay well within the alowable limit of $1.0\mu g$.

The effect of aerodynamic torque was also considered. The torque model accounts for the diurnal bulge at twice the orbital rate. Now, the TEA shifts from $\psi_e = 1.5°, \lambda_e = \phi_e = 0°$, to $\psi_e = 13°, \lambda_e = 9°$ and $\phi_e = 7°$. This change in equilibrium reflected in an increase in the control effort (from $Q_\psi = 1$ Nm, $Q_\lambda = Q_\phi = 0$ Nm to $Q_\psi = 4.5$ Nm, $Q_\lambda = 1.5$ Nm, and $Q_\phi = 1.4$ Nm). The solar panels and secondary members do not exhibit any significant change in behaviour, with similar responses as before in displacement and acceleration.

To summarize, rotation of the solar panels for tracking the sun, even in the presence of aerodynamic drag, is not likely to affect the microgravity experiments. Furthermore, the control effort required to maintain the spacecraft in the LVLH orientation is rather minimal.

4.3 MSS Operational Maneuvers

The Mobile Servicing System (MSS) manipulator arm, among other tasks, will be used to position payloads along the Space Station's main truss. Here it is proposed to investigate a maneuver designed specifically for this purpose. Consider the case where a disabled satellite has been retrieved by the Space Shuttle and delivered to the Space Station docking bay, and it is to be transferred to the maintenance depot for repair. To accomplish this task, the manipulator is commanded to perform a series of slewing and translational maneuvers. The maneuver consists of three distinct steps: (i) a 90° slewing motion in the plane of the solar panels, divided into four 22.5° increments. Each increment follows a sine-on-ramp profile; (ii) a translation of 22.5 m along the main truss, divided into five steps; and finally (iii) a 90° rotation to position the satellite at the the root of the solar panels, with the slewing motion

composed of $4 \times 22.5°$ steps.

The manipulator is modelled by a single arm 15 meters in length, and uniformly distributed mass of 3,200 kgs, carrying a 3,200 Kgs payload at the end.

The maneuver has been discretized into ten time steps ($t_1 \rightarrow t_{10}$). During this task, the frequency spectrum undergoes significant frequency excursions in modes 11, 20, 23, 24 and 25, with changes in frequency as large as 30% in mode 20 (Figure 6a). Furthermore, the associated modal displacements also exhibited considerable changes during the maneuver as well. For example, mode 25 displays a transfer of modal energy, in this case from the manipulator arm to the PV radiator. Mode 11 started by having the strain energy stored in bending of the solar panels and PV radiator, at time step t_5 the RCS boom and stinger displayed predominant modal motion, and by the end of the maneuver t_{10} the elastic energy reverted back to the PV radiator and solar arrays. Mode 20 displayed a very interesting behaviour; at the beginning of the maneuver, the motion of the main truss, at its free end, was suppressed by the presence of the robot arm, which acts effectively as an added inertia on an anti-node of a free-free beam. When the arm reaches a modal node in the main truss (t_6), the main truss motion shows large modal displacements since the mass damper is unable to influence the main truss motion.

The ensuing dynamic response simulation is presented in Figure 6b. The various maneuvers are well demarked in the plots. It can be observed that the slewing maneuvers exert considerable disturbance to the Station environment compared to the translation maneuvers. The complete positioning task lasts 0.225 orbit (22.5 minutes). The inplane slewing of the MSS arm exerts a moment about the local vertical; this torque is transmitted to the Space Station, which in turn is counteracted by the CMGs with a corresponding peak control effort in the yaw degree of freedom ($Q_\lambda = 1014.5$ Nm). The MSS arm displays a maximum transverse tip displacement of 3×10^{-4} m with corresponding acceleration of $5\mu g$. The acceleration levels around the modules on the main truss were found to be quite high (10 μg).

Simulations were also carried out for a 1,000 kgs payload. It was observed that the control efforts and acceleration levels at various Station location decreased considerably (50%).

5. CONCLUDING REMARKS

Applicability and versatility of a general Lagrangian formulation are illustrated through the analysis of the First Milestone Configuration of the proposed Space Station. Predicting the dynamic response of the Space Station to disturbances encountered during normal operation are an important step in the process of defining design loads for the main truss structure, as well as for the modules and secondary components. The control effort profile to maintain the LVLH attitude orientation of the Station, the displacement and acceleration response time histories for several

locations were presented for each case and the peak response values were tabulated for comparison. The dynamic analysis results indicate that the solar array sun track maneuvers caused accelerations on the order of 0.1 μg, and the MSS positioning operation resulted in peak acceleration of 10 μg at the laboratory module attachment point on the main truss.

6. REFERENCES

1. Suleman, A., *Dynamics and Control of Evolving Space Platforms: A Formulation with Applications*, Ph.D. Thesis, University of British Columbia, Vancouver, Canada, August 1992.
2. Freund, E., "The Structure of Decoupled Nonlinear Systems", *International Journal of Control*, Vol. 21, No. 3, 1975, pp. 443-450.
3. Beijczy, A.K., *Robot Arm Dynamics and Control*, JPL TM 33-669, California Institute of Technology, Pasadena, California, 1974.
4. Singh, S.N., and Schy, A.A., "Invertibility and Robust Nonlinear Control of Robotic Systems", *Proceedings of the 23rd Conference on Decision and Control*, Las Vega, Nevada, December 1984, pp. 1058-1063.
5. Spong, M.W., and Vidyasagar, M., "Robust Linear Compensator Design for Nonlinear Robotic Control", *Proceedings of IEEE Conference on Decision and Control*, Fort Lauderdale, florida, December 1985, pp. 1767-1772.
6. Hunt, L.R., Su, R., and Meyer, G., "Global Transformations of Nonlinear Systems", *IEEE Transactions of Automatic Control*, Vol. AC-28, 1983, pp. 24-31.
7. Karray, F., Modi, V.J., and Chan, J.K., "Nonlinear Modelling and Dynamic Feedback of the Flexible Remote Manipulator System", *Proceedings of the 1991 American Control Conference*, Boston, USA, Editor: A.G. Ulsoy, Vol. 3, pp. 1909-1912.

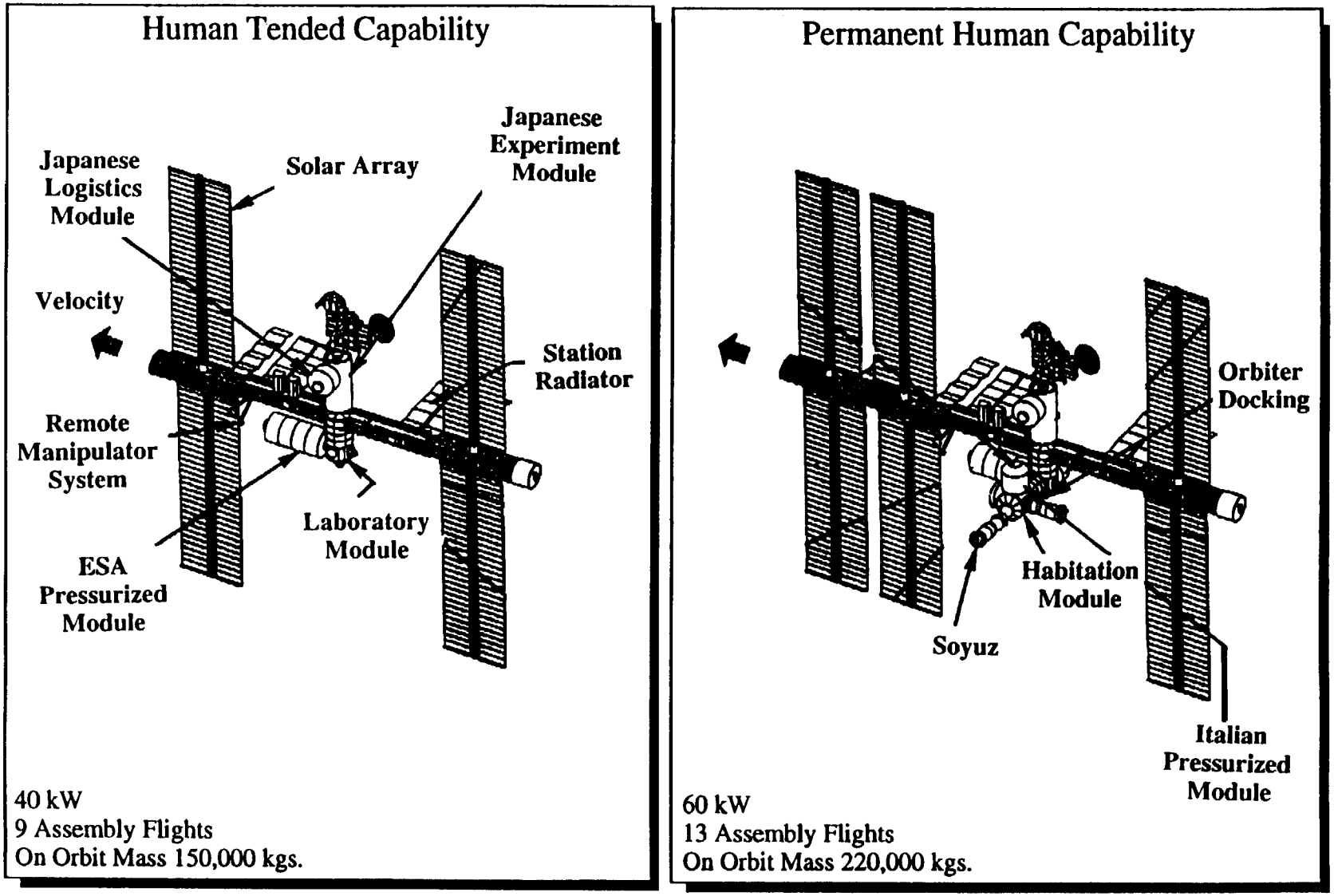

Figure 1 Proposed Space Station *Freedom* redesigned configurations as of June 1993 showing the Human Tended and the Permanent Human Capabilities.

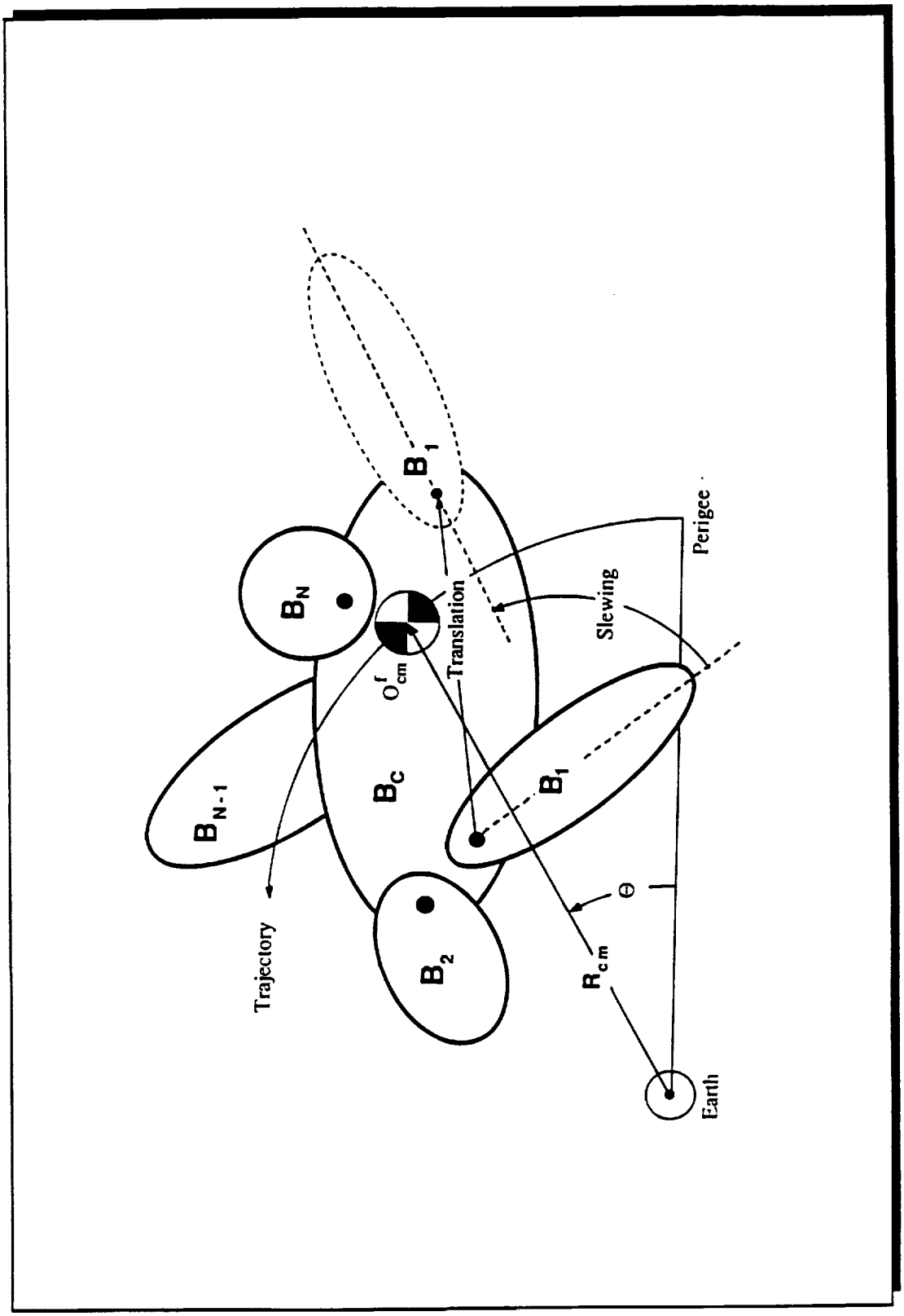

Figure 2 A schematic diagram of the multibody space structure in an open tree configuration.

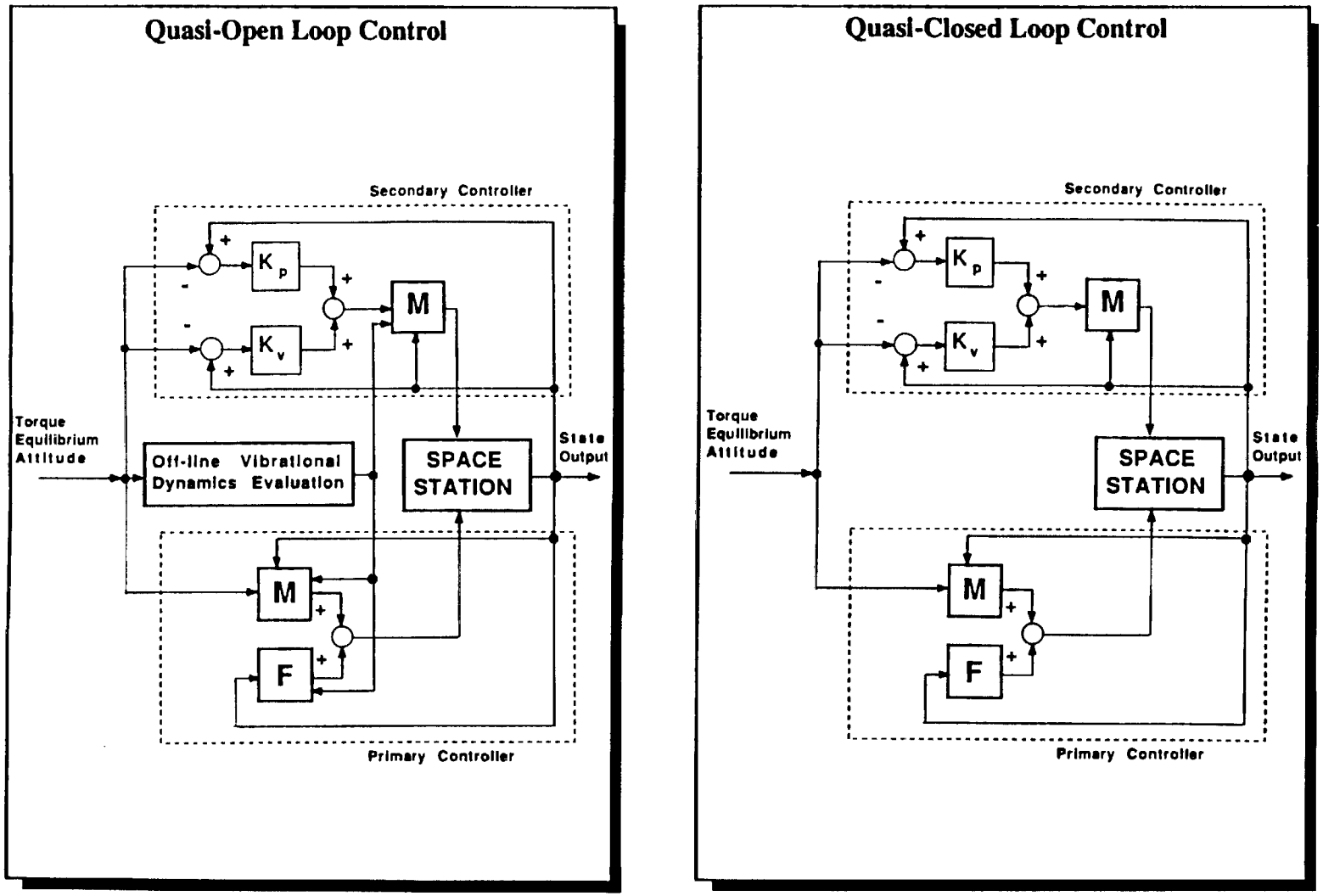

Figure 3 Block diagram for the nonlinear attitude control strategy using the Feedback Linearization Technique: (a) Quasi-Open Loop Technique; and (b) Quasi-Closed Loop Technique.

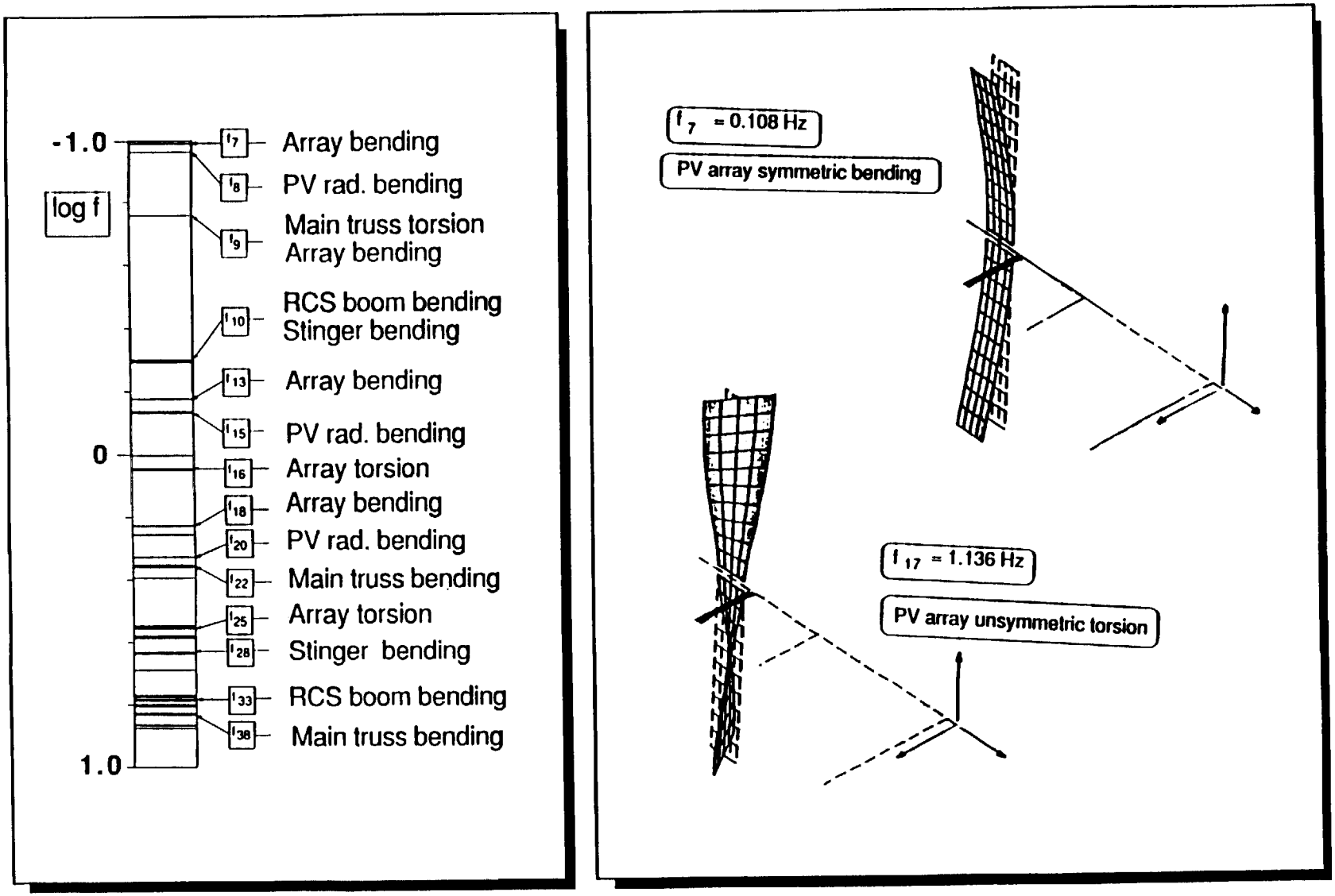

Figure 4 Frequency spectrum and mode shapes for the First Milestone Configuration of the Space Station showing a closely spaced and overlapping character.

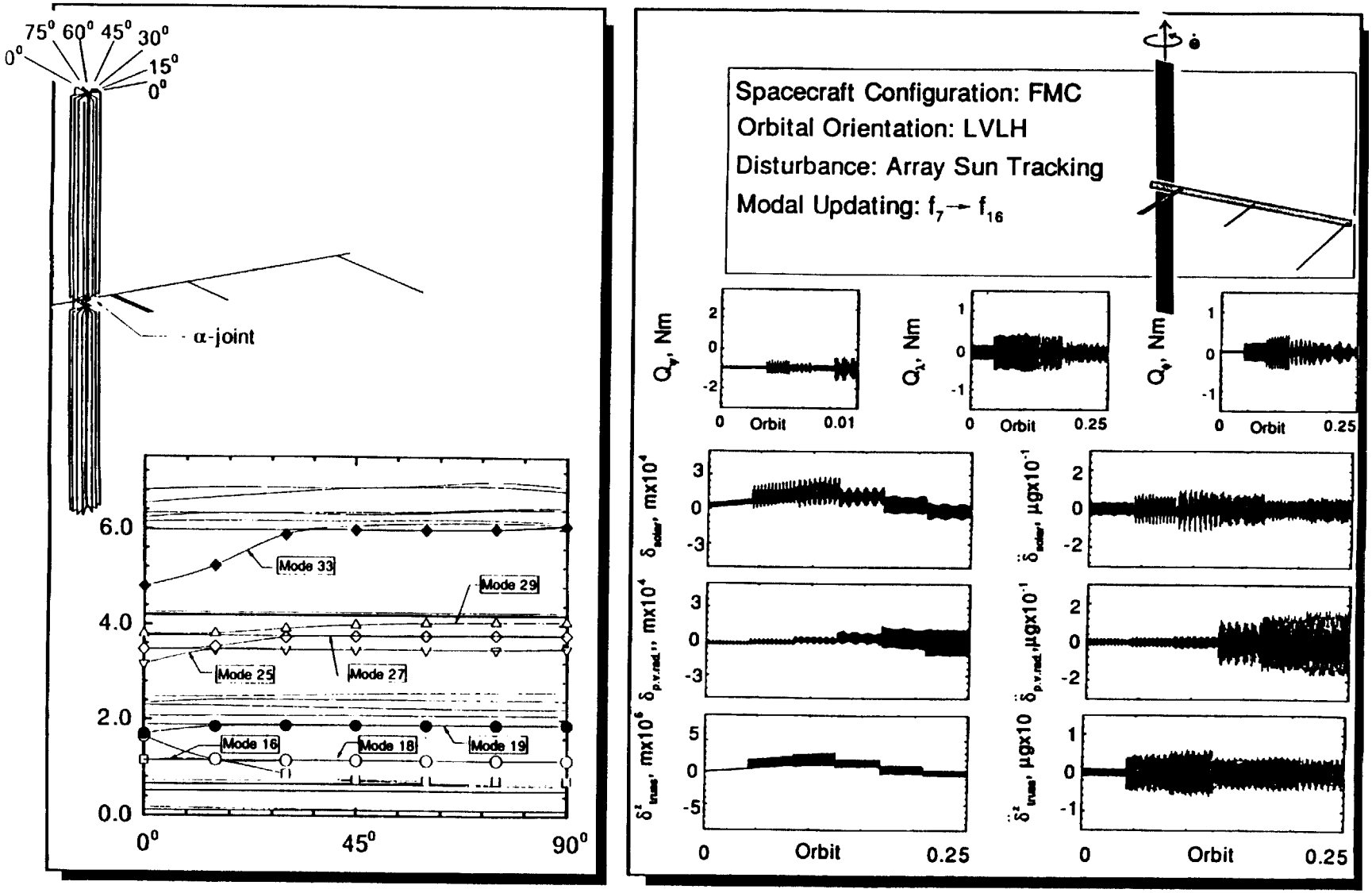

Figure 5 The Space Station response to the solar panels rotation to track the sun for optimum exposure: (a) the frequency spectrum showing the updated modal information at 15 degree intervals to maintain an accurate representation of the system geometry and deformation; and (b) the control effort, and the displacement and acceleration time histories for critical locations on the Space Station.

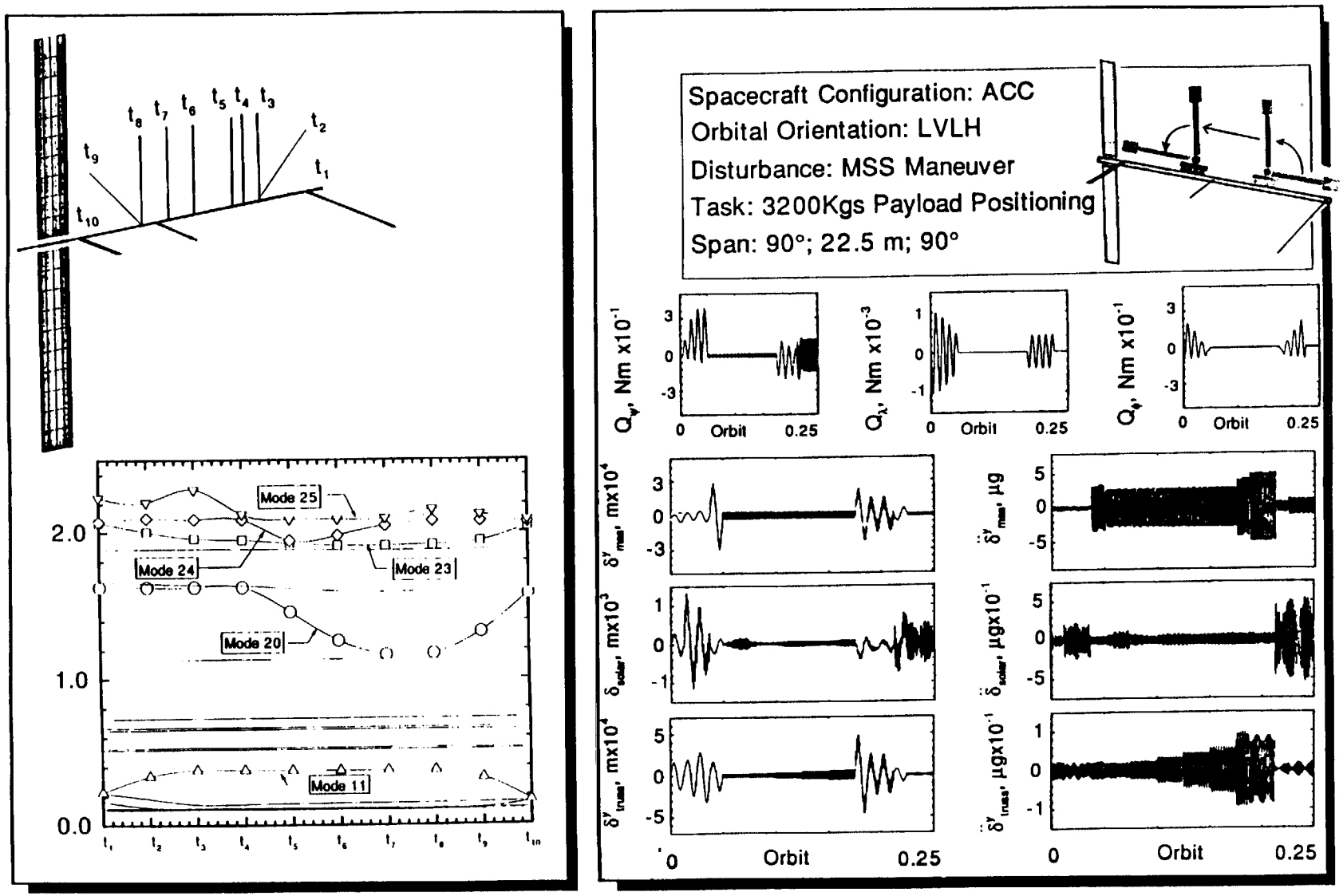

Figure 6 The dynamical response of the Space Station in the presence of the MSS payload positioning maneuver: (a) the spectrum depicting the frequency excursions during the maneuver at 10 time steps; and (b) the control effort, and the displacement and acceleration time histories for the tip of the MSS and solar panels and the location of the laboratory module on the main truss during the maneuver.